

Generating Einstein-Podolsky-Rosen correlations for teleporting collective spin states in a two-dimensional trapped ion crystal

Muhammad Miskeen Khan ^{1,2} Edwin Chaparro ^{1,2} Bhuvanesh Sundar ^{1,*} Allison Carter ³
John Bollinger ³ Klaus Molmer ⁴ and Ana Maria Rey ^{1,2}

¹*JILA, National Institute of Standards and Technology and University of Colorado, 440 UCB, Boulder, Colorado 80309, USA*

²*Center for Theory of Quantum Matter, University of Colorado, Boulder, Colorado 80309, USA*

³*National Institute of Standards and Technology, Boulder, Colorado 80309, USA*

⁴*Niels Bohr Institute, University of Copenhagen, 2100 Copenhagen, Denmark*



(Received 21 June 2024; accepted 5 March 2025; published 17 April 2025)

We propose the use of phonon-mediated interactions as an entanglement resource to engineer Einstein-Podolsky-Rosen correlations and to perform teleportation of collective spin states in two-dimensional ion crystals. We emulate continuous variable quantum teleportation protocols between subsystems corresponding to different nuclear spin degrees of freedom. In each of them, a quantum state is encoded in an electronic spin degree of freedom that couples to the vibrational modes of the crystal. We show that high fidelity teleportation of spin-coherent states and their phase-displaced variant, entangled spin-squeezed states, and Dicke states, is possible for realistic experimental conditions in arrays from a few tens to a few hundred ions.

DOI: [10.1103/PhysRevResearch.7.L022019](https://doi.org/10.1103/PhysRevResearch.7.L022019)

Introduction. Correlated quantum states, such as entangled spin-squeezed states, have been predicted to offer a significant gain in sensing and communication applications [1]. While great progress has been achieved using macroscopic atomic ensembles in optical cavities or vapor cells [2–11], these systems typically lack the level of quantum control over motional degrees of freedom desired for more general quantum information tasks. Arrays of two-dimensional trapped-ion crystals [12–18] are emerging as a promising platform where one can scale up the number of ions while retaining full or partial quantum control over vibrational modes and all-to-all internal state connectivity. These capabilities can thus open an exciting opportunity for entanglement generation using collective spin systems. In the context of quantum information processing, quantum teleportation is one of the most useful resources [19–27] that unravels the power of entanglement for quantum communication [28,29], protection of quantum information [30,31], transduction and energy transport [32,33], testing information scrambling with its connections to quantum gravity [34–39], and implementing quantum computing modules [40–42]. While teleportation of optical and spin coherent states have been experimentally demonstrated using large atomic ensembles [43,44], teleportation of collective entangled spin states in trapped ion platforms that enjoy control over both internal and external degrees of freedom

[36,45,46], as required for most quantum information processing tasks, is still pending. Here we demonstrate that quantum teleportation of collective spin-states can be implemented in current two-dimensional (2D) crystal arrays in a Penning trap using the center-of-mass motional mode as an entanglement resource. The proposed scheme is analogous to the continuous variable quantum teleportation scheme of Braunstein and Kimble (BK) [21], however, instead of relying on measurement based schemes for entanglement generation [47], our system uses unitary phonon-mediated all-to-all spin-spin interactions. Measurements, enabled by spectroscopic resolution of internal spin levels of ions, are only used for the act of teleportation [44] at the end of the protocol. The access to long-range spin-spin interactions in trapped ion arrays [12,45] allows for the initialization of entangled states [13], which we show can also be teleported. Our proposed model thus opens a path for studying quantum information processing with multilevel collective spin systems by employing multipartite entanglement. Additionally, it enables implementation of continuous variable quantum information protocols [48] without the overhead of additional nonlinearities, which are typically engineered under carefully controlled conditions in pure phononic systems [49–51]. Moreover, since the phonon modes in trapped-ion systems are very long-lived, our system does not suffer from the detrimental losses faced by photons. Finally, while we focus here on states within the same spatial ensemble, the applicability of the same protocols in bilayer arrays or 3D crystals [52] could enable the possibility to teleport states between spatially separated layers.

Setup. We consider a 2D trapped ion crystal made of $^9\text{Be}^+$ ions in a Penning trap as schematically shown in Fig. 1(a). The crystal is located in the X - Y plane and it is subjected to a strong magnetic field ($B \sim 4.5$ T) along the Z – direction that sets the quantization axis and allows us to work in the

*Present address: Rigetti Computing, 775 Heinz Avenue, Berkeley, California 94710, USA.

Published by the American Physical Society under the terms of the Creative Commons Attribution 4.0 International license. Further distribution of this work must maintain attribution to the author(s) and the published article's title, journal citation, and DOI.

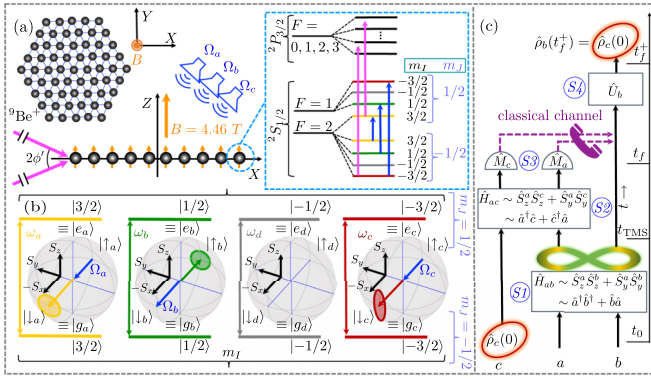


FIG. 1. (a) Schematic for a two-dimensional trapped ion crystal made of ${}^9\text{Be}^+$ ions located in the (X, Y) plane as realized in the Penning trap at NIST [53]. A strong magnetic field B results in splitting of the internal Zeeman levels as shown in the inset. The nuclear spins form distinctly addressable ensembles $l = a, b, c$. An optical dipole force (ODF) implemented by Raman beams [pink] couples each nuclear spin ensemble to a common transverse vibrational mode of the ions. Three spin ensembles are resonantly driven by microwaves with Rabi frequencies Ω_l , $l = \{a, b, c\}$, to implement the teleportation circuit. (b) The initial states of the nuclear spin ensemble are shown on the corresponding Bloch spheres. From left to right, spin ensembles a [yellow] and b [green] are initialized along $-S_x$ and $+S_x$ directions, respectively, with circular noise distributions representing their initial spin-coherent states. The ensemble c [red] is initialized along $-S_x$ direction with its elliptical noise distribution representing an input spin-squeezed state. (c) Schematics of the teleportation protocol: it consists of different stages ($S1$ - $S4$) as discussed in the text. The times for dynamical processes are given by $t_f = t_{\text{TMS}} + t_{\text{BS}}$ (see also text), and $t_f^+ = t_f + t_{\text{CL}}$, where t_{CL} is the duration to receive classically communicated measurement results and performing local rotations on ensemble b .

Paschen-Back regime [54] with decoupled electronic (with $J = 1/2$) and nuclear (with $I = 3/2$) hyperfine-Zeeman states as shown in the inset of the Fig. 1(a). In our scheme, the ions are initialized in three out of a total four nuclear spin states [55], $m_l = 3/2 (l = a)$, $1/2 (l = b)$, $-3/2 (l = c)$, with $N_{l=a,b,c}$ ions in each nuclear spin ensemble. In this way we have access to three distinct choices of qubit degrees of freedom per atom, each one characterized by the $\{|e_l\rangle, |g_l\rangle\}$ levels with energy splitting ω_l , where the labels g, e denote the $m_J = -1/2, 1/2$ electronic states respectively. Thanks to the large energy separation, $\omega_{ll'} \equiv \omega_l - \omega_{l'} \sim 500$ MHz [55], the different nuclear spin subensembles can be independently controlled with negligible coupling between them by microwave drives, with Rabi drive strength Ω_l and frequency ω_l^D , as schematically shown in Fig. 1(b).

We further assume the ions are driven by interfering laser beams with a beat-note frequency μ as shown in Fig. 1(a). The beams are applied off-resonantly (detuned by ~ 20 GHz) to the nearest optical transition spanned by the ${}^2P_{3/2}$ manifold. Their polarization and orientation are set to couple the spin degree of freedom to the axial modes of the crystal and μ is set to be close to the center-of-mass (COM) mode frequency of the crystal, ω_M to avoid excitation of other modes [cf. inset of Fig. 1(a)]. The net result is the generation of an electronic-spin-dependent optical dipole force (ODF) on the

ions [12] that acts approximately in the opposite direction for the $m_J = \pm 1/2$ states [up to a small correction ϵ_l which turns out to be irrelevant for the physics in consideration (see Ref. [56])].

Assuming the motion of the ions has an axial extent that is small compared to the wavelength of the moving lattice, by going to the rotating frame of the beat-note frequency, the Hamiltonian of the total system can be written as ($\hbar = 1$):

$$\hat{H} = \hat{H}_s + \hat{H}_{\text{ODF}}, \quad (1)$$

$\hat{H}_s = \sum_{l=a,b,c} [\omega_l \hat{S}_z^l + \Omega_l/2 (\hat{S}_+^l e^{-i\omega_l^D t} + \text{H.c.})]$ describes the applied microwave drives and $\hat{H}_{\text{ODF}} = \delta_M \hat{m}^\dagger \hat{m} + \sum_{l=a,b,c} \frac{g_l}{\sqrt{N}} (\hat{m} + \hat{m}^\dagger) \hat{S}_z^l$ the ODF Hamiltonian with $\delta_M = \omega_M - \mu$ [57]. Here, we introduced the COM phonon annihilation (creation) operator $\hat{m} (\hat{m}^\dagger)$ and $S_\alpha^l \equiv \frac{1}{2} \sum_{j=1}^{N_l} \sigma_\alpha^{l,j}$ the collective spin operators, with $\alpha = (x, y, z)$ and $\hat{S}_\pm^l \equiv \hat{S}_x^l \pm i \hat{S}_y^l$ the corresponding raising and lowering operators. The spin-phonon coupling is denoted by g_l , and $N = \sum_l N_l$ is the total number of ions in the crystal. Note that the values N_l are set by the initial preparation and they are conserved during the interaction of the ions. For each ensemble, the single ion coupling g_l is inversely proportional to the one-photon Raman detuning, and thus can be slightly different for each of the nuclear spin ensembles by the order of just a few percent.

In a frame rotating at the microwave drive frequency, resonant with the nuclear spin transition $\omega_l = \omega_l^D$, we rewrite the Hamiltonian \hat{H} in the dressed (rotated) basis. The dressed states are eigenstates of the microwave drives, and are explicitly given by $|\uparrow_l\rangle = (|g_l\rangle + |e_l\rangle)/\sqrt{2}$ and $|\downarrow_l\rangle = (|g_l\rangle - |e_l\rangle)/\sqrt{2}$ as shown in Fig. 1(b) on the corresponding Bloch spheres. In terms of the collective spin operators in the dressed frame ($-\hat{S}_x^l \rightarrow \hat{S}_z^l$, $\hat{S}_y^l \rightarrow \hat{S}_y^l$, $\hat{S}_z^l \rightarrow \hat{S}_x^l$), the Hamiltonian reads [57]

$$\hat{H} = \sum_l \Omega_l \hat{S}_z^l - \sum_l \frac{g_l}{\sqrt{N}} (\hat{m} + \hat{m}^\dagger) \hat{S}_x^l + \delta_M \hat{m}^\dagger \hat{m}. \quad (2)$$

We further consider the special case where the spin ensembles a, b, c are initially spin-polarized [56] along $-S_x$, $+S_x$ and $-S_x$ direction of their corresponding Bloch sphere, respectively [see Fig. 1(b)]. Following such initialization, the ensemble c is subjected to a unitary operation that transforms the state into a spin coherent state (which can also be slightly displaced from the initial mean magnetization), a spin squeezed state, or a Dicke state [58–60]. This is the state we aim to teleport. We implement the teleportation protocol consisting of different stages ($S1$ - $S4$) as outlined in Fig. 1(c), involving an entangling operation ($S1$) between a and b ensembles, followed by a beam-splitter ($S2$) interaction between a and c ensembles. The outcomes of the measurement performed ($S3$) on the latter two are then classically communicated to ensemble b , enabling us to perform spin rotations ($S4$) on ensemble b to retrieve the teleported state.

Teleportation protocol. For the first stage of the teleportation protocol, we set $\Omega_c = 0$ in Eq. (2), since we do not want ions in this state to participate in the dynamics. Assuming that $|\Delta_M^{ab}| \equiv |\delta_M - \Omega_{ab}| \gg g_l$, with $\Omega_{ab} \equiv (\Omega_a + \Omega_b)/2$ and $\delta_{ab} \equiv (\Omega_a - \Omega_b)/2$ we can adiabatically eliminate the COM phonon mode. By going to a rotating frame defined by the

unitary transformation $U = e^{i\Omega_{ab}(\hat{S}_z^a + \hat{S}_z^b + \hat{m}^\dagger \hat{m})t}$, we obtain an effective spin-spin interaction Hamiltonian of the form [56]:

$$\begin{aligned} \hat{H}_{ab} = & -\chi_{ab}(\hat{S}_+^a \hat{S}_-^b + \hat{S}_-^a \hat{S}_+^b) \\ & -\chi_{aa}\hat{S}_z^a \hat{S}_z^a - \chi_{bb}\hat{S}_z^b \hat{S}_z^b + \delta_{ab}(\hat{S}_z^a - \hat{S}_z^b). \end{aligned} \quad (3)$$

Here $\chi_{\alpha\alpha'} \equiv (g_\alpha g_{\alpha'})/(4\bar{N}\Delta_M^{ab})$, with $\{\alpha, \alpha'\} \in \{a, b\}$. The first line in Eq. (3) describes flip-flop processes between the two different spin ensembles. The second line, up to constants of motion that we have omitted, includes the self-interaction terms plus an energy shift arising from the two different Rabi frequencies. We wish to employ this Hamiltonian to generate correlated excitations between the ensembles a and b . To do so, as mentioned above, we initialize the a, b ensembles in fully polarized states with opposite magnetization, e.g., in eigenstates of \hat{S}_z^a and \hat{S}_z^b with eigenvalues $-N_a/2$ and $N_b/2$, respectively. When \hat{H}_{ab} is applied to these states, the flip-flop term $\hat{S}_+^a \hat{S}_-^b$ simultaneously generates a spin $|\uparrow_a\rangle$ excitation in the a ensemble and a spin $|\downarrow_b\rangle$ excitation in the b ensemble as desired. This process, however, imposes an energy cost of $\chi_{aa}N_a + \chi_{bb}N_b$ arising from the self-interactions. This energy penalty can be compensated by an appropriate choice of the Rabi frequencies driving the a, b ensembles. Specifically by setting $\delta_{ab} = \chi_{aa}N_a = \chi_{bb}N_b \equiv \bar{\chi}\bar{N}$ one can approximately cancel the energy penalty [56]. The above discussion is valid in $N_a \sim N_b \gg 1$ limit, where we can use the mean-field approximation (i.e., $\hat{O}\hat{R} \rightarrow \hat{O}\langle\hat{R}\rangle + \hat{R}\langle\hat{O}\rangle - \langle\hat{O}\rangle\langle\hat{R}\rangle$) and approximate $\hat{S}_z^a \hat{S}_z^a \approx 2\langle\hat{S}_z^a\rangle\hat{S}_z^a = -N_a\hat{S}_z^a$ and $\hat{S}_z^b \hat{S}_z^b \approx 2\langle\hat{S}_z^b\rangle\hat{S}_z^b = N_b\hat{S}_z^b$ plus constant terms.

To mathematically formalize the excitation process, we utilize the Holstein-Primakoff (HP) transformation and approximate the collective spin operators by bosonic operators: $\hat{S}_+^a \simeq \sqrt{N_a}\hat{a}^\dagger$, $\hat{S}_+^c \simeq \sqrt{N_c}\hat{c}^\dagger$ and $\hat{S}_+^b \simeq \sqrt{N_b}\hat{b}$ up to leading order in $1/N_{a,b,c}$, such that $\hat{S}_x^l \approx \sqrt{N_l}/2\hat{X}_l$, $\hat{S}_y^{a,c} \approx -\sqrt{N_{a,c}}/2\hat{P}_{a,c}$ and $\hat{S}_y^b \approx \sqrt{N_b}/2\hat{P}_b$. Here we have defined $\hat{X}_l = \frac{1}{\sqrt{2}}(\hat{l} + \hat{l}^\dagger)$, $\hat{P}_l = \frac{1}{i\sqrt{2}}(\hat{l} - \hat{l}^\dagger)$, which satisfy the standard commutation relation $[\hat{X}_l, \hat{P}_l] = i$ for $l = a, b, c$ and simplify the spin-exchange Hamiltonian to a two-mode squeezing (TMS) interaction that generates correlations between two bosonic modes [8,56]:

$$\hat{H}_{\text{TMS}} \approx -\chi_{ab}\bar{N}[\hat{a}^\dagger \hat{b}^\dagger + \hat{b}\hat{a}] \quad (4)$$

with $\bar{N} \sim N_a \sim N_b$. The correlated creation of pairs of spin excitations from the initial state results in a thermofield double (TFD) state of the form $|\psi_{ab}\rangle = (1/\cosh r) \sum_{n=0}^{\infty} (-i)^n \tanh^n r |n, n\rangle$. Here $r \equiv \bar{N}\chi_{ab}t$ is the magnitude of the two-mode squeezing parameter determined by the interaction time [61]. The TFD state features an exponential growth and attenuation of the bosonic hybrid quadratures defined as $\hat{X}^\mp \equiv (\hat{P}_b \pm \hat{X}_a)/\sqrt{2}$ and $\hat{P}^\pm \equiv (\hat{X}_b \pm \hat{P}_a)/\sqrt{2}$, so $\hat{X}^\mp(t) = \hat{X}^\mp(0)e^{\pm\bar{N}\chi_{ab}t}$ and $\hat{P}^\pm(t) = \hat{P}^\pm(0)e^{\pm\bar{N}\chi_{ab}t}$. For $\chi_{ab} < 0$ and in the ideal case of infinitely large interaction time, one reaches the Einstein-Podolsky-Rosen (EPR) conditions [62,63], $\hat{P}_b^{\text{ideal}} = -\hat{X}_a^{\text{ideal}}$ and $\hat{X}_b^{\text{ideal}} = -\hat{P}_a^{\text{ideal}}$, or in terms of the spin variables (assuming the validity of HP with $\bar{N} \rightarrow \infty$),

$$\hat{S}_y^{\text{ideal},b} - \hat{S}_z^{\text{ideal},a} = 0, \quad \hat{S}_y^{\text{ideal},a} + \hat{S}_z^{\text{ideal},b} = 0 \quad (5)$$

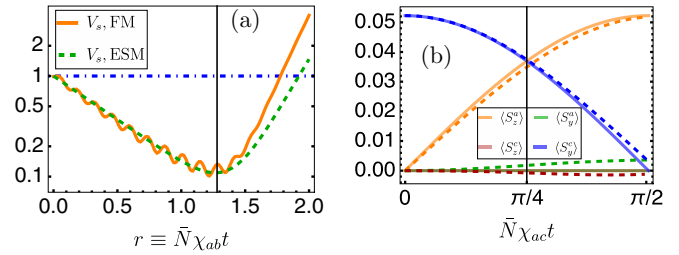


FIG. 2. (a) Entanglement parameter V_s [Eq. (6)] as a function of $r = \bar{N}\chi_{ab}t$ with t the interaction time. Orange solid and green dashed lines represent the full model (FM) and effective spin model (ESM) dynamics. (b) Beam-splitter step: Dashed and corresponding solid lines show the dynamics obtained under the ESM and HP approximations, respectively. The vertical black lines in (a) and (b) correspond to interaction times where the TMS and BS operation are truncated, respectively. Throughout our analysis, we assume parameters $\Omega_a = \Omega_c = -2\pi \times 19.1$ kHz, $\Omega_b = -2\pi \times 18.8$ kHz, $g_a = g_b = g_c = 2\pi \times 3.6$ kHz, and $\delta_M/(2\pi) = -26$ kHz. The dynamics is simulated with $N_a = N_b = N_c = \bar{N} = 70$.

Thus, in such an ideal limit, their variances $V[\cdot]$ become negligible, $V[\hat{S}_y^{\text{ideal},b} - \hat{S}_z^{\text{ideal},a}] \rightarrow 0$ and $V[\hat{S}_y^{\text{ideal},a} + \hat{S}_z^{\text{ideal},b}] \rightarrow 0$. Away from the ideal case, the development of entanglement, in terms of spin operators, can be witnessed by the inequality

$$V_s \equiv \frac{V[\hat{S}_y^b - \hat{S}_z^a] + V[\hat{S}_z^b + \hat{S}_y^a]}{|\langle\hat{S}_x^a\rangle| + |\langle\hat{S}_x^b\rangle|} < 1, \quad (6)$$

which serves as an entanglement witness [64–66]. In Fig. 2(a), we plot V_s with increasing r both for the full model (FM) under the Hamiltonian in Eq. (2) and the effective spin model (ESM) described by Eq. (3). The entanglement between the a and b ensembles starts building up as soon as the interaction becomes operational. The maximum entanglement is achieved at $r = r_{\text{min}} \equiv \bar{N}\chi_{ab}t_{\text{TMS}}$, the point where V_s is minimum. For $t > t_{\text{TMS}}$ finite size effects start playing a role and as V_s increases above its minimum value, and it is no longer a useful quantifier of the entanglement.

Following the BK teleportation scheme [21], setting t_{TMS} when V_s is optimal, the next step is to engineer an effective beam-splitter (BS) operation. We again start from the spin/phonon Hamiltonian in Eq. (2) but at this stage of the protocol, we set $\Omega_b = 0$, since we want to freeze the dynamics in the state of ensemble b . Akin to the previous stage, we adiabatically eliminate the phonon mode and go to a rotating frame, now set by $U = e^{if_r(\hat{S}_z^a + \hat{S}_z^c + \hat{m}^\dagger \hat{m})t}$, where f_r , a frequency that depends on system parameters, can be chosen such that we obtain only a BS operation (see below). This rotating frame leads to an equation similar to Eq. (3), and we again obtain an effective spin-spin interaction, but with c replacing b . In contrast to the prior case, we now want to initialize ensemble c with a large spin projection along the same direction as a , e.g., with most of the ions aligned along the south pole of the dressed c Bloch sphere. Under this condition, when \hat{H}_{ac} is applied to the joint state, the flip-flop term $\hat{S}_-^a \hat{S}_+^c$ transfers a spin excitation $|\uparrow_a\rangle$ in the a ensemble to a spin $|\uparrow_c\rangle$ excitation in the c ensemble and vice versa for the $\hat{S}_+^a \hat{S}_-^c$ term, as desired for a BS. Note that in this case the self-interactions do not generate an energy penalty. Nevertheless, they can induce a

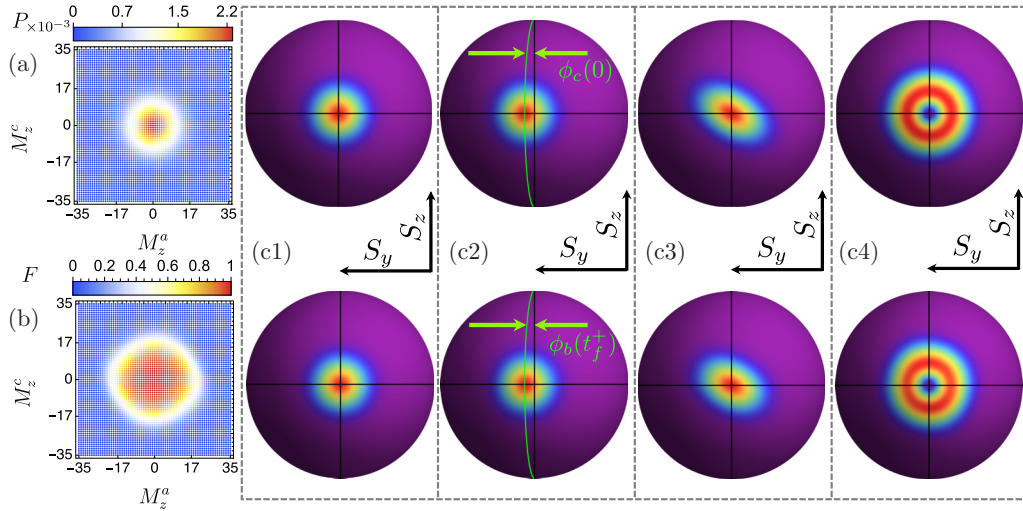


FIG. 3. (a) Measurement outcome probability distribution function $P(M_z^a, M_z^c)$ of an input spin-coherent state. More examples are shown in Ref. [56]. (b) Teleportation fidelity for different measurement outcomes. (c) Top row: the Husimi-Q function of SC, PDSC, SS, and DS (with $k_c = 1$) input states, respectively. Bottom row: Husimi-Q function of teleported states.

small self-generated precession of the collective spins in the a, c ensembles that we want to ideally remove. So we set $\Omega_a = \Omega_c$, and adjust f_r to approximately cancel it (see Ref. [56]). In the HP approximation limit, the effective interaction between the a and c bosons reads now [56]:

$$\hat{H}_{BS} = -\chi_{ac}\bar{N}[\hat{a}^\dagger\hat{c} + \hat{c}^\dagger\hat{a}]. \quad (7)$$

Here we defined the effective mode frequency $\Delta_M^{ac} = \delta_M - f_r$ and assumed $\chi_{aa}N_a \sim \chi_{cc}N_c \equiv \bar{\chi}\bar{N}$, and $N_a \sim N_c \sim \bar{N}$. To realize the required 50-50 BS operation, the BS Hamiltonian is applied for a time $\bar{N}\chi_{ac}t_{BS} = \pi/4$ (Fig. 2(b), i.e., when ensemble c is slightly displaced from the initial mean magnetization).

As a result at $t_f = t_{BS} + t_{TMS}$, we obtain $\hat{S}_z^a(t_f) = (\hat{S}_z^a(0) + \hat{S}_z^a(t_{TMS}))/\sqrt{2}$ and $\hat{S}_z^c(t_f) = (\hat{S}_z^c(0) + \hat{S}_y^a(t_{TMS}))/\sqrt{2}$. Projective measurements to infer z -components of the a and c ensembles then cause a collapse according to $\hat{S}_z^a(t_{TMS}) = \beta_z - \hat{S}_y^a(0)$ and $\hat{S}_y^a(t_{TMS}) = \beta_y - \hat{S}_z^c(0)$, with $\beta_z/\sqrt{2} = M_z^a \equiv (k_a - N_a/2)$ and $\beta_y/\sqrt{2} = M_z^c \equiv (k_c - N_c/2)$, the measured outcomes where $k_{a,c}$ are the number of excitations in the spin ensembles. Ideally, due to the EPR property in Eq. (5), the state of ensemble b is immediately projected according to, $\hat{S}_y^{\text{ideal},b}(t_f) = \sqrt{2}M_z^a(t_f) - \hat{S}_y^a(0)$ and $\hat{S}_z^{\text{ideal},b}(t_f) = -\sqrt{2}M_z^c(t_f) + \hat{S}_z^c(0)$.

These equations reflect that the projected state of ensemble b is simply a ‘‘rotated’’ state of the input state of the ensemble c . By employing our knowledge of the measurement outcomes $M_z^{a,c}$, we can apply rotations of ensemble b given by $\hat{U}_b = \hat{D}_\pi \hat{D}_r(\beta_y, \beta_z)$, where $\hat{D}_r(\beta_y, \beta_z) = \exp[i(2/N_b)(\beta_z \hat{S}_z^b + \beta_y \hat{S}_y^b)]$ [56], and $\hat{D}_\pi = \exp(i\pi \hat{S}_z^b)$, which complete the desired teleportation.

Numerical calculations. We numerically simulate the many body spin-ensemble teleportation protocol using exact diagonalization (ED). In Fig. 3(a) we show the results when the input state $\hat{\rho}_c(0)$ is a spin-coherent state for which the most probable outcome is $\beta_y = 0, \beta_z = 0$. To

compare the teleported state $\hat{\rho}_b(t_f^+)$ to the input state for the most probable outcome, in Fig. 3(c), we plot the Husimi-Q functions, i.e., $Q(\theta, \phi) \equiv (1/4\pi)\langle \psi_{SC}(\theta, \phi) | \hat{\rho}_c(0) | \psi_{SC}(\theta, \phi) \rangle$ of four different input states of c given by a spin coherent state $|\psi_{SC}(\pi/2, \pi)\rangle$ (SC), a phase-displaced spin coherent $\exp(-i\phi_c \hat{S}_z^c) |\psi_{SC}(\pi/2, \pi)\rangle$ (PDSC), a spin-squeezed state, $|\psi_{SS}\rangle = \exp(-i\phi_{ss}(\hat{S}_z^c)^2) |\psi_{SC}(\pi/2, \pi)\rangle$ (SS), and a Dicke state, $|\psi_{DS}\rangle = \exp(-i[\pi/2]\hat{S}_y^c)\hat{S}_+^c |\psi_{SC}(\pi, 0)\rangle$ (DS) with one excitation. Here $|\psi_{SC}(\theta, \phi)\rangle$ represents a generic spin coherent state [67]. The Dicke state is included here to show that the teleportation protocol applies also for such states, while we note that their preparation as input states would need a higher order nonlinearity or a heralding protocol [68]. We also show (bottom row) their teleported versions. For all cases, the mean orientations and noise distributions of the teleported states match the ones of the input. To make a more quantitative comparison, we compute the Uhlmann fidelity $F(M_z^a, M_z^c) = [\text{Tr}(\sqrt{\sqrt{\hat{\rho}_c(0)}\hat{\rho}_b(t_f^+)\sqrt{\hat{\rho}_c(0)}})]^2$ [69] between the input and teleported SC states for different measurement outcomes and show it in Fig. 3(b) for $N_a = N_b = N_c = \bar{N} = 70$. Similar results are shown for PDSC, SS, and DS states in Ref. [56].

For the most probable outcomes $\tilde{M}_z^a, \tilde{M}_z^c$, the fidelities are given by $F_{SC}(\tilde{M}_z^a, \tilde{M}_z^c) = F_{PDSC}(\tilde{M}_z^a, \tilde{M}_z^c) = 0.99$, $F_{SS}(\tilde{M}_z^a, \tilde{M}_z^c) = 0.98$, and $F_{DS}(\tilde{M}_z^a, \tilde{M}_z^c) = 0.99$. With the current protocol, for an input phase $\phi_c(0) = 6^\circ$, we obtain a teleported state with a phase $\phi_b(t_f^+) = 5.34^\circ$. For the SS states we obtain a squeezing parameter $\xi_b(t_f^+) = -3.17$ (dB), for an input state with $\xi_c(0) = -4.15$ (dB). The errors are limited by curvature corrections due to finite ion number. For the average fidelity $\bar{F} = \sum_{M_z^a, M_z^c} P(M_z^a, M_z^c) F(M_z^a, M_z^c)$ we obtain the averages fidelities to be $\bar{F}_{SC} = \bar{F}_{PDSC} = 0.87$, $\bar{F}_{SS} = 0.85$, and $\bar{F}_{DS} = 0.68$ for the corresponding input states with $\bar{N} = 70$.

To further assess how the available entanglement affects the performance of the teleportation, we plot the average fidelity as a function of r up to r_{\min} for a fixed number of ions N_l

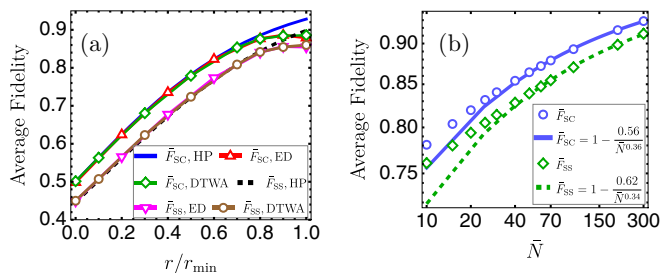


FIG. 4. (a) Numerically computed average teleportation fidelity for SC and SS input states as a function of entangling interaction time $r = \bar{N}\chi_{abt}$. The entangling time is increased until $r = r_{\min}$, time at which entanglement witness is optimal for $\bar{N} = 70$. (b) The average teleportation fidelity scaling with the number of ions \bar{N} for SC and SS input states.

as shown in Fig. 4(a). We numerically average the fidelity both with the ED and the discrete truncated Wigner approximation methods [56]. As expected, there is a monotonic increase in the average fidelity against r both for the SC and SS states and the fidelity closely follows the analytic expression obtained with the HP solution [56,70–72] at short times. For longer times, finite size effects are reduced by increasing \bar{N} (see Ref. [56]). In Fig. 4(b) we compute the average fidelity scaling with \bar{N} for the SC and SS cases. We find a scaling $\bar{F}_{SC} \simeq 1 - [0.56/(\bar{N}^{0.36})]$ and $\bar{F}_{SS} \simeq 1 - [0.62/(\bar{N}^{0.34})]$.

Experimental considerations. Many of the necessary ingredients for the protocol have been individually demonstrated already in Penning traps: Population of various nuclear spins levels using rf pulses have been achieved in ${}^9\text{Be}^+$ [55]. Global subensemble rotations enjoy fidelities as high as 99%. The COM mode has been cooled down close to its ground state value [73] and the observed phonon damping rate γ_m is mostly irrelevant. Since the dominant decoherence channel is single spin dephasing induced by Rayleigh and Raman scattering with rates $\Gamma_{RI} > \Gamma_{Rm}$ [57] the main limitation is the requirement $\Gamma_{RI}t_{TMS} < V_s$, $t_{BS}\Gamma_{RI} \ll 1$ and $t_f\Gamma_{RI} < \xi_c(0)$. For current experimental parameters $g_a \sim g_b \sim g_c \approx 2\pi \times 4$ kHz, $\bar{N} \approx 70$ and $\Gamma_{RI} \approx 250$ s $^{-1}$, we expect to achieve a TMS parameter $r \approx 0.55$ and therefore an average teleportation fidelity of $\bar{F} \approx 0.75$ for a coherent state and $\bar{F} \approx 0.65$ for a SS state with $\xi_c(0) \approx -5.3$ dB.

Fluorescence measurements have been also demonstrated [13] for a single nuclear spin component $m_I = \pm 3/2$ prepared via optical pumping [12,74]. Even though the collection efficiency in current experiments may be just at the threshold needed to avoid errors from off resonant light scattering into other nuclear spin states during detection, in the future, improved detection efficiency can be gained by using high-aperture lenses or a build-up cavity. Alternatively, instead of nuclear spins, an additional narrow optical transition enabled by optical-metastable-ground-states [75–78], could significantly enhance the detection fidelity. For example, instead of ${}^9\text{Be}^+$, one can use ${}^{43}\text{Ca}^+$, and during the measurement step, transfer the qubits to the ${}^2D_{5/2}$ level.

Outlook. While in this work we have focused on how to achieve entanglement generation and teleportation in a

trapped ion architecture, our scheme can be implemented in any system featuring collective spin-spin interactions. For example, it could be realized in arrays of ${}^{87}\text{Sr}$ atoms inside an optical cavity where all 10 nuclear spin ground levels can be coupled to the long-lived metastable 3P_0 or 3P_1 states via photon exchange. In this system all the ten transitions can be independently addressed as demonstrated in clock experiments [79]. Besides the elastic interactions, one will need to account for the inelastic interactions arising from the finite lifetime of the cavity photons, but as explained in Ref. [8], as long as the collective cooperativity is high, teleportation should be possible. Alternatively instead of long-lived internal levels, addressable momentum states can be used as a pseudospin degree of freedom, as recently experimentally demonstrated in optical cavities with Rb atoms [80,81]. Another relevant type of system where our protocol could be implemented is an array of polar molecules, or magnetic atoms, with rotational or hyperfine states coupled by dipolar exchange interactions, and prepared in separate layers as experimentally reported [82–84]. While dipolar interactions are not genuinely all-to-all, by engineering Heisenberg interactions via floquet pulses in mobile molecules [85] or via electric field control in pinned arrays [86], one can effectively make the interactions collective as numerically studied in Ref. [87] and experimentally confirmed in dipolar systems [85,86].

Another direction to pursue and complement current work, is to take advantage of long-lived phonon modes, which can be cooled down in current experiments, as extra active channels. The hybrid spin-phonon architecture can offer even broader capabilities. One specific advantage is faster preparation time scales compared to the pure spin case discussed here, and thus less sensitivity to decoherence with the only overhead being an additional transfer operation between the phonon mode and a spin degree of freedom for readout [88].

Finally, while we have focused on spins in the same spatial ensemble, teleportation between spatially separated ensembles could be achieved in crystal bilayers or 3D crystals [52] by using the addressable sections of the crystal as collective spin degrees of freedom. Furthermore, five effective channels, e.g., four nuclear spin sub-ensembles and one active phonon mode, opens also the exciting possibility to implement protocols to disentangle scrambling and decoherence via quantum teleportation [36–38]. Beyond teleportation, similar schemes could be used for retroactive squeezing generation and enhanced displacement sensing in the Penning trap [5].

Acknowledgments. We thank R. Kaubruegger and J. Lilieholm for their useful feedback on the manuscript and D. Wellnitz for helpful discussions. This material is based upon work supported by the Heising-Simons foundation and the U.S. Department of Energy, Office of Science, National Quantum Information Science Research Centers, Quantum Systems Accelerator. We also acknowledge funding support from ARO Grant No. W911NF24-1-0128, the NSF JILA-PFC PHY-2317149, AFOSR Grant No. FA9550-25-1-0080, and NIST. K.M. acknowledges the Carlsberg Foundation through the “Semper Ardens” Research Project QCool.

- [1] L. Pezzè, A. Smerzi, M. K. Oberthaler, R. Schmied, and P. Treutlein, Quantum metrology with nonclassical states of atomic ensembles, *Rev. Mod. Phys.* **90**, 035005 (2018).
- [2] O. Hosten, N. J. Engelsen, R. Krishnakumar, and M. A. Kasevich, Measurement noise 100 times lower than the quantum-projection limit using entangled atoms, *Nature (London)* **529**, 505 (2016).
- [3] K. C. Cox, G. P. Greve, J. M. Weiner, and J. K. Thompson, Deterministic squeezed states with collective measurements and feedback, *Phys. Rev. Lett.* **116**, 093602 (2016).
- [4] J. Appel, P. J. Windpassinger, D. Oblak, U. B. Hoff, N. Kjærgaard, and E. S. Polzik, Mesoscopic atomic entanglement for precision measurements beyond the standard quantum limit, *Proc. Natl. Acad. Sci. USA* **106**, 10960 (2009).
- [5] H. Bao, J. Duan, S. Jin, X. Lu, P. Li, W. Qu, M. Wang, I. Novikova, E. E. Mikhailov, K.-F. Zhao, K. Mølmer, H. Shen, and Y. Xiao, Spin squeezing of 1011 atoms by prediction and retrodiction measurements, *Nature (London)* **581**, 159 (2020).
- [6] S. Colombo, E. Pedrozo-Peñafiel, A. F. Adiyatullin, Z. Li, E. Mendez, C. Shu, and V. Vuletić, Time-reversal-based quantum metrology with many-body entangled states, *Nat. Phys.* **18**, 925 (2022).
- [7] J. M. Robinson, M. Miklos, Y. M. Tso, C. J. Kennedy, T. Bothwell, D. Kedar, J. K. Thompson, and J. Ye, Direct comparison of two spin-squeezed optical clock ensembles at the 10–17 level, *Nat. Phys.* **20**, 208 (2024).
- [8] B. Sundar, D. Barberena, A. P. n. Orioli, A. Chu, J. K. Thompson, A. M. Rey, and R. J. Lewis-Swan, Bosonic pair production and squeezing for optical phase measurements in long-lived dipoles coupled to a cavity, *Phys. Rev. Lett.* **130**, 113202 (2023).
- [9] E. S. Cooper, P. Kunkel, A. Periwal, and M. Schleier-Smith, Graph states of atomic ensembles engineered by photon-mediated entanglement, *Nat. Phys.* **20**, 770 (2024).
- [10] P. Colciaghi, Y. Li, P. Treutlein, and T. Zibold, Einstein-Podolsky-Rosen experiment with two Bose-Einstein condensates, *Phys. Rev. X* **13**, 021031 (2023).
- [11] G. Bornet, G. Emperauger, C. Chen, B. Ye, M. Block, M. Bintz, J. A. Boyd, D. Barredo, T. Comparin, F. Mezzacapo, T. Roscilde, T. Lahaye, N. Y. Yao, and A. Browaeys, Scalable spin squeezing in a dipolar Rydberg atom array, *Nature (London)* **621**, 728 (2023).
- [12] J. W. Britton, B. C. Sawyer, A. C. Keith, C.-C. J. Wang, J. K. Freericks, H. Uys, M. J. Biercuk, and J. J. Bollinger, Engineered two-dimensional Ising interactions in a trapped-ion quantum simulator with hundreds of spins, *Nature (London)* **484**, 489 (2012).
- [13] J. G. Bohnet, B. C. Sawyer, J. W. Britton, M. L. Wall, A. M. Rey, M. Foss-Feig, and J. J. Bollinger, Quantum spin dynamics and entanglement generation with hundreds of trapped ions, *Science* **352**, 1297 (2016).
- [14] M. Gärttner, J. G. Bohnet, A. Safavi-Naini, M. L. Wall, J. J. Bollinger, and A. M. Rey, Measuring out-of-time-order correlations and multiple quantum spectra in a trapped-ion quantum magnet, *Nat. Phys.* **13**, 781 (2017).
- [15] K. A. Gilmore, M. Affolter, R. J. Lewis-Swan, D. Barberena, E. Jordan, A. M. Rey, and J. J. Bollinger, Quantum-enhanced sensing of displacements and electric fields with two-dimensional trapped-ion crystals, *Science* **373**, 673 (2021).
- [16] S. Mavadia, J. F. Goodwin, G. Stutter, S. Bharadia, D. R. Crick, D. M. Segal, and R. C. Thompson, Control of the conformations of ion Coulomb crystals in a penning trap, *Nat. Commun.* **4**, 2571 (2013).
- [17] D. Kiesenhofer, H. Hainzer, A. Zhdanov, P. C. Holz, M. Bock, T. Ollikainen, and C. F. Roos, Controlling two-dimensional Coulomb crystals of more than 100 ions in a monolithic radio-frequency trap, *PRX Quantum* **4**, 020317 (2023).
- [18] S.-A. Guo, Y.-K. Wu, J. Ye, L. Zhang, W.-Q. Lian, R. Yao, Y. Wang, R.-Y. Yan, Y.-J. Yi, Y.-L. Xu, B.-W. Li, Y.-H. Hou, Y.-Z. Xu, W.-X. Guo, C. Zhang, B.-X. Qi, Z.-C. Zhou, L. He, and L.-M. Duan, A site-resolved two-dimensional quantum simulator with hundreds of trapped ions, *Nature (London)* **630**, 613 (2024).
- [19] C. H. Bennett, G. Brassard, C. Crépeau, R. Jozsa, A. Peres, and W. K. Wootters, Teleporting an unknown quantum state via dual classical and Einstein-Podolsky-Rosen channels, *Phys. Rev. Lett.* **70**, 1895 (1993).
- [20] L. Vaidman, Teleportation of quantum states, *Phys. Rev. A* **49**, 1473 (1994).
- [21] S. L. Braunstein and H. J. Kimble, Teleportation of continuous quantum variables, *Phys. Rev. Lett.* **80**, 869 (1998).
- [22] B. K. Rugg, M. D. Krzyaniak, B. T. Phelan, M. A. Ratner, R. M. Young, and M. R. Wasielewski, Photodriven quantum teleportation of an electron spin state in a covalent donor-acceptor-radical system, *Nat. Chem.* **11**, 981 (2019).
- [23] M. D. Barrett, J. Chiaverini, T. Schaetz, J. Britton, W. M. Itano, J. D. Jost, E. Knill, C. Langer, D. Leibfried, R. Ozeri, and D. J. Wineland, Deterministic quantum teleportation of atomic qubits, *Nature (London)* **429**, 737 (2004).
- [24] S. Olmschenk, D. N. Matsukevich, P. Maunz, D. Hayes, L.-M. Duan, and C. Monroe, Quantum teleportation between distant matter qubits, *Science* **323**, 486 (2009).
- [25] M. Riebe, H. Häffner, C. F. Roos, W. Hänsel, J. Benhelm, G. P. T. Lancaster, T. W. Körber, C. Becher, F. Schmidt-Kaler, D. F. V. James, and R. Blatt, Deterministic quantum teleportation with atoms, *Nature (London)* **429**, 734 (2004).
- [26] S. Pirandola, J. Eisert, C. Weedbrook, A. Furusawa, and S. L. Braunstein, Advances in quantum teleportation, *Nat. Photon.* **9**, 641 (2015).
- [27] X.-M. Hu, Y. Guo, B.-H. Liu, C.-F. Li, and G.-C. Guo, Progress in quantum teleportation, *Nat. Rev. Phys.* **5**, 339 (2023).
- [28] R. Valivarathi, M. G. Puigibert, Q. Zhou, G. H. Aguilar, V. B. Verma, F. Marsili, M. D. Shaw, S. W. Nam, D. Oblak, and W. Tittel, Quantum teleportation across a metropolitan fibre network, *Nat. Photon.* **10**, 676 (2016).
- [29] J.-G. Ren, P. Xu, H.-L. Yong, L. Zhang, S.-K. Liao, J. Yin, W.-Y. Liu, W.-Q. Cai, M. Yang, L. Li, K.-X. Yang, X. Han, Y.-Q. Yao, J. Li, H.-Y. Wu, S. Wan, L. Liu, D.-Q. Liu, Y.-W. Kuang, Z.-P. He *et al.*, Ground-to-satellite quantum teleportation, *Nature (London)* **549**, 70 (2017).
- [30] Y.-H. Luo, M.-C. Chen, M. Erhard, H.-S. Zhong, D. Wu, H.-Y. Tang, Q. Zhao, X.-L. Wang, K. Fujii, L. Li, N.-L. Liu, K. Nemoto, W. J. Munro, C.-Y. Lu, A. Zeilinger, and J.-W. Pan, Quantum teleportation of physical qubits into logical code spaces, *Proc. Natl. Acad. Sci. USA* **118**, e2026250118 (2021).
- [31] F. Eckstein, B. Han, S. Trebst, and G.-Y. Zhu, Robust teleportation of a surface code and cascade of topological quantum phase transitions, *PRX Quantum* **5**, 040313 (2024).

- [32] J. Wu, C. Cui, L. Fan, and Q. Zhuang, Deterministic microwave-optical transduction based on quantum teleportation, *Phys. Rev. Appl.* **16**, 064044 (2021).
- [33] K. Ikeda, Demonstration of quantum energy teleportation on superconducting quantum hardware, *Phys. Rev. Appl.* **20**, 024051 (2023).
- [34] T. Schuster, B. Kobrin, P. Gao, I. Cong, E. T. Khabiboulline, N. M. Linke, M. D. Lukin, C. Monroe, B. Yoshida, and N. Y. Yao, Many-body quantum teleportation via operator spreading in the traversable wormhole protocol, *Phys. Rev. X* **12**, 031013 (2022).
- [35] S. Nezami, H. W. Lin, A. R. Brown, H. Gharibyan, S. Leichenauer, G. Salton, L. Susskind, B. Swingle, and M. Walter, Quantum gravity in the lab. II. Teleportation by size and traversable wormholes, *PRX Quantum* **4**, 010321 (2023).
- [36] K. A. Landsman, C. Figgatt, T. Schuster, N. M. Linke, B. Yoshida, N. Y. Yao, and C. Monroe, Verified quantum information scrambling, *Nature (London)* **567**, 61 (2019).
- [37] M. S. Blok, V. V. Ramasesh, T. Schuster, K. O'Brien, J. M. Kreikebaum, D. Dahlen, A. Morvan, B. Yoshida, N. Y. Yao, and I. Siddiqi, Quantum information scrambling on a superconducting qutrit processor, *Phys. Rev. X* **11**, 021010 (2021).
- [38] B. Yoshida and N. Y. Yao, Disentangling scrambling and decoherence via quantum teleportation, *Phys. Rev. X* **9**, 011006 (2019).
- [39] S. Antonini, B. Grado-White, S.-K. Jian, and B. Swingle, Holographic measurement and quantum teleportation in the SYK thermofield double, *J. High Energy Phys.* **02** (2023) 095.
- [40] D. Gottesman and I. L. Chuang, Demonstrating the viability of universal quantum computation using teleportation and single-qubit operations, *Nature (London)* **402**, 390 (1999).
- [41] W.-B. Gao, A. M. Goebel, C.-Y. Lu, H.-N. Dai, C. Wagenknecht, Q. Zhang, B. Zhao, C.-Z. Peng, Z.-B. Chen, Y.-A. Chen, and J.-W. Pan, Teleportation-based realization of an optical quantum two-qubit entangling gate, *Proc. Natl. Acad. Sci. USA* **107**, 20869 (2010).
- [42] K. S. Chou, J. Z. Blumoff, C. S. Wang, P. C. Reinhold, C. J. Axline, Y. Y. Gao, L. Frunzio, M. H. Devoret, L. Jiang, and R. J. Schoelkopf, Deterministic teleportation of a quantum gate between two logical qubits, *Nature (London)* **561**, 368 (2018).
- [43] H. Krauter, D. Salart, C. A. Muschik, J. M. Petersen, H. Shen, T. Fernholz, and E. S. Polzik, Deterministic quantum teleportation between distant atomic objects, *Nat. Phys.* **9**, 400 (2013).
- [44] J. F. Sherson, H. Krauter, R. K. Olsson, B. Julsgaard, K. Hammerer, I. Cirac, and E. S. Polzik, Quantum teleportation between light and matter, *Nature (London)* **443**, 557 (2006).
- [45] C. Monroe, W. C. Campbell, L.-M. Duan, Z.-X. Gong, A. V. Gorshkov, P. W. Hess, R. Islam, K. Kim, N. M. Linke, G. Pagano, P. Richerme, C. Senko, and N. Y. Yao, Programmable quantum simulations of spin systems with trapped ions, *Rev. Mod. Phys.* **93**, 025001 (2021).
- [46] Y. Wan, D. KiENZler, S. D. Erickson, K. H. Mayer, T. R. Tan, J. J. Wu, H. M. Vasconcelos, S. Glancy, E. Knill, D. J. Wineland, A. C. Wilson, and D. Leibfried, Quantum gate teleportation between separated qubits in a trapped-ion processor, *Science* **364**, 875 (2019).
- [47] L.-M. Duan, J. I. Cirac, P. Zoller, and E. S. Polzik, Quantum communication between atomic ensembles using coherent light, *Phys. Rev. Lett.* **85**, 5643 (2000).
- [48] S. L. Braunstein and P. van Loock, Quantum information with continuous variables, *Rev. Mod. Phys.* **77**, 513 (2005).
- [49] R. T. Sutherland and R. Srinivas, Universal hybrid quantum computing in trapped ions, *Phys. Rev. A* **104**, 032609 (2021).
- [50] J. Metzner, A. Quinn, S. Brudney, I. D. Moore, S. C. Burd, D. J. Wineland, and D. T. C. Allcock, Two-mode squeezing and SU(1,1) interferometry with trapped ions, *Phys. Rev. A* **110**, 022613 (2024).
- [51] O. Katz and C. Monroe, Programmable quantum simulations of bosonic systems with trapped ions, *Phys. Rev. Lett.* **131**, 033604 (2023).
- [52] S. Hawaldar, P. Shahi, A. L. Carter, A. M. Rey, J. J. Bollinger, and A. Shankar, Bilayer crystals of trapped ions for quantum information processing, *Phys. Rev. X* **14**, 031030 (2024).
- [53] J. J. Bollinger, J. W. Britton, and B. C. Sawyer, Simulating quantum magnetism with correlated non-neutral ion plasmas, *AIP Conf. Proc.* **1521**, 200 (2013).
- [54] G. Herzberg, *Atomic Spectra and Atomic Structure* (Dover Publications, New York, 1944).
- [55] N. Shiga, W. M. Itano, and J. J. Bollinger, Diamagnetic correction to the $^9\text{Be}^+$ ground-state hyperfine constant, *Phys. Rev. A* **84**, 012510 (2011).
- [56] See Supplemental Material at <http://link.aps.org/supplemental/10.1103/PhysRevResearch.7.L022019> for the detail derivations and supportive numerical results for the main text.
- [57] A. Safavi-Naini, R. J. Lewis-Swan, J. G. Bohnet, M. Gärtner, K. A. Gilmore, J. E. Jordan, J. Cohn, J. K. Freericks, A. M. Rey, and J. J. Bollinger, Verification of a many-ion simulator of the Dicke model through slow quenches across a phase transition, *Phys. Rev. Lett.* **121**, 040503 (2018).
- [58] Y. O. Dudin, L. Li, F. Bariani, and A. Kuzmich, Observation of coherent many-body Rabi oscillations, *Nat. Phys.* **8**, 790 (2012).
- [59] J. Lee, M. J. Martin, Y.-Y. Jau, T. Keating, I. H. Deutsch, and G. W. Biedermann, Demonstration of the Jaynes-Cummings ladder with Rydberg-dressed atoms, *Phys. Rev. A* **95**, 041801(R) (2017).
- [60] J. Zeiher, R. van Bijnen, P. Schauf, S. Hild, J.-y. Choi, T. Pohl, I. Bloch, and C. Gross, Many-body interferometry of a Rydberg-dressed spin lattice, *Nat. Phys.* **12**, 1095 (2016).
- [61] C. Weedbrook, S. Pirandola, R. García-Patrón, N. J. Cerf, T. C. Ralph, J. H. Shapiro, and S. Lloyd, Gaussian quantum information, *Rev. Mod. Phys.* **84**, 621 (2012).
- [62] A. Serafini, *Quantum Continuous Variables: A Primer of Theoretical Methods* (CRC Press, Boca Raton, Florida, 2017).
- [63] A. Einstein, B. Podolsky, and N. Rosen, Can quantum-mechanical description of physical reality be considered complete? *Phys. Rev.* **47**, 777 (1935).
- [64] V. Giovannetti, S. Mancini, D. Vitali, and P. Tombesi, Characterizing the entanglement of bipartite quantum systems, *Phys. Rev. A* **67**, 022320 (2003).
- [65] L.-M. Duan, G. Giedke, J. I. Cirac, and P. Zoller, Inseparability criterion for continuous variable systems, *Phys. Rev. Lett.* **84**, 2722 (2000).
- [66] B. Julsgaard, A. Kozhekin, and E. S. Polzik, Experimental long-lived entanglement of two macroscopic objects, *Nature (London)* **413**, 400 (2001).
- [67] J. Ma, X. Wang, C. Sun, and F. Nori, Quantum spin squeezing, *Phys. Rep.* **509**, 89 (2011).

- [68] R. McConnell, H. Zhang, J. Hu, S. Ćuk, and V. Vuletić, Entanglement with negative Wigner function of almost 3,000 atoms heralded by one photon, *Nature (London)* **519**, 439 (2015).
- [69] R. Jozsa, Fidelity for mixed quantum states, *J. Mod. Opt.* **41**, 2315 (1994).
- [70] A. Mari and D. Vitali, Optimal fidelity of teleportation of coherent states and entanglement, *Phys. Rev. A* **78**, 062340 (2008).
- [71] Z. Li, C. mei Liu, J. L. Wang, and M. Zhang, The quantum teleportation fidelity of the squeezed vacuum state, in *Proceedings of the 2015 International Conference on Automation, Mechanical Control and Computational Engineering* (Atlantis Press, Dordrecht, 2015).
- [72] A. V. Chizhov, L. Knöll, and D.-G. Welsch, Continuous-variable quantum teleportation through lossy channels, *Phys. Rev. A* **65**, 022310 (2002).
- [73] E. Jordan, K. A. Gilmore, A. Shankar, A. Safavi-Naini, J. G. Bohnet, M. J. Holland, and J. J. Bollinger, Near ground-state cooling of two-dimensional trapped-ion crystals with more than 100 ions, *Phys. Rev. Lett.* **122**, 053603 (2019).
- [74] D. J. Wineland, J. C. Bergquist, W. M. Itano, and R. E. Drullinger, Double-resonance and optical-pumping experiments on electromagnetically confined, laser-cooled ions, *Opt. Lett.* **5**, 245 (1980).
- [75] D. T. C. Allcock, W. C. Campbell, J. Chiaverini, I. L. Chuang, E. R. Hudson, I. D. Moore, A. Ransford, C. Roman, J. M. Sage, and D. J. Wineland, *omg* blueprint for trapped ion quantum computing with metastable states, *Appl. Phys. Lett.* **119**, 214002 (2021).
- [76] H.-X. Yang, J.-Y. Ma, Y.-K. Wu, Y. Wang, M.-M. Cao, W.-X. Guo, Y.-Y. Huang, L. Feng, Z.-C. Zhou, and L.-M. Duan, Realizing coherently convertible dual-type qubits with the same ion species, *Nat. Phys.* **18**, 1058 (2022).
- [77] O. Băzăvan, S. Saner, M. Minder, A. C. Hughes, R. T. Sutherland, D. M. Lucas, R. Srinivas, and C. J. Ballance, Synthesizing a $\hat{\sigma}_z$ spin-dependent force for optical, metastable, and ground-state trapped-ion qubits, *Phys. Rev. A* **107**, 022617 (2023).
- [78] B. J. McMahon, K. R. Brown, C. D. Herold, and B. C. Sawyer, Individual-ion addressing and readout in a penning trap, *Phys. Rev. Lett.* **133**, 173201 (2024).
- [79] M. M. Boyd, T. Zelevinsky, A. D. Ludlow, S. M. Foreman, S. Blatt, T. Ido, and J. Ye, Optical atomic coherence at the 1-second time scale, *Science* **314**, 1430 (2006).
- [80] C. Luo, H. Zhang, V. P. W. Koh, J. D. Wilson, A. Chu, M. J. Holland, A. M. Rey, and J. K. Thompson, Momentum-exchange interactions in a Bragg atom interferometer suppress doppler dephasing, *Science* **384**, 551 (2024).
- [81] C. Luo, H. Zhang, C. Maruko, E. A. Bohr, A. Chu, A. M. Rey, and J. K. Thompson, Realization of three and four-body interactions between momentum states in a cavity through optical dressing, [arXiv:2410.12132](https://arxiv.org/abs/2410.12132).
- [82] W. G. Tobias, K. Matsuda, J.-R. Li, C. Miller, A. N. Carroll, T. Bilitewski, A. M. Rey, and J. Ye, Reactions between layer-resolved molecules mediated by dipolar spin exchange, *Science* **375**, 1299 (2022).
- [83] P. Barral, M. Cantara, L. Du, W. Lunden, J. de Hond, A. O. Jamison, and W. Ketterle, Suppressing dipolar relaxation in thin layers of dysprosium atoms, *Nat. Commun.* **15**, 3566 (2024).
- [84] A. Douglas, V. Kaxiras, L. Su, M. Szurek, V. Singh, O. Marković, and M. Greiner, Spin squeezing with magnetic dipoles, [arXiv:2411.07219](https://arxiv.org/abs/2411.07219).
- [85] C. Miller, A. N. Carroll, J. Lin, H. Hirzler, H. Gao, H. Zhou, M. D. Lukin, and J. Ye, Two-axis twisting using floquet-engineered XYZ spin models with polar molecules, *Nature (London)* **633**, 332 (2024).
- [86] A. N. Carroll, H. Hirzler, C. Miller, D. Wellnitz, S. R. Muleady, J. Lin, K. P. ZamarSKI, R. R. W. Wang, J. L. Bohn, A. M. Rey, and J. Ye, Observation of generalized t-j spin dynamics with tunable dipolar interactions, [arXiv:2404.18916](https://arxiv.org/abs/2404.18916).
- [87] T. Bilitewski and A. M. Rey, Manipulating growth and propagation of correlations in dipolar multilayers: From pair production to bosonic Kitaev models, *Phys. Rev. Lett.* **131**, 053001 (2023).
- [88] R. J. Lewis-Swan, J. C. Zuniga Castro, D. Barberena, and A. M. Rey, Exploiting nonclassical motion of a trapped ion crystal for quantum-enhanced metrology of global and differential spin rotations, *Phys. Rev. Lett.* **132**, 163601 (2024).